Article

Soil–Water Dynamics Investigation at Agricultural Hillslope with High-Precision Weighing Lysimeters and Soil–Water Collection Systems

Vedran Krevh [1,*], Jannis Groh [2,3,4], Lana Filipović [1], Horst H. Gerke [4], Jasmina Defterdarović [1], Sally Thompson [5], Mario Sraka [6], Igor Bogunović [7], Zoran Kovač [8], Nathan Robinson [9], Thomas Baumgartl [10] and Vilim Filipović [1,10]

[1] Department of Soil Amelioration, Faculty of Agriculture, University of Zagreb, 10000 Zagreb, Croatia
[2] Institute of Crop Science and Resource Conservation—Soil Science and Soil Ecology, University of Bonn, 53113 Bonn, Germany
[3] Forschungszentrum Jülich GmbH, Institute of Bio- and Geoscience (IBG-3, Agrosphere), 52428 Jülich, Germany
[4] Leibniz Centre for Agricultural Landscape Research (ZALF), Research Area 1 "Landscape Functioning", 5374 Müncheberg, Germany
[5] School of Engineering, Civil, Environmental and Mining Engineering, University of Western Australia, Perth, WA 6009, Australia
[6] Department of Soil Science, Faculty of Agriculture, University of Zagreb, 10000 Zagreb, Croatia
[7] Department of General Agronomy, Faculty of Agriculture, University of Zagreb, 10000 Zagreb, Croatia
[8] Department of Geology and Geological Engineering, Faculty of Mining Geology and Petroleum Engineering, University of Zagreb, 10000 Zagreb, Croatia
[9] Centre for eResearch and Digital Innovation, Federation University, Mount Helen, VIC 3350, Australia
[10] Future Regions Research Centre, Geotechnical and Hydrogeological Engineering Research Group, Federation University, Gippsland, VIC 3841, Australia
[*] Correspondence: vkrevh@agr.hr

Abstract: A quantitative understanding of actual evapotranspiration (ET_a) and soil–water dynamics in a hillslope agroecosystem is vital for sustainable water resource management and soil conservation; however, the complexity of processes and conditions involving lateral subsurface flow (LSF) can be a limiting factor in the full comprehension of hillslope soil–water dynamics. The research was carried out at SUPREHILL CZO located on a hillslope agroecosystem (vineyard) over a period of two years (2021–2022) by combining soil characterization and field hydrological measurements, including weighing lysimeters, sensor measurements, and LSF collection system measurements. Lysimeters were placed on the hilltop and the footslope, both having a dynamic controlled bottom boundary, which corresponded to field pressure head measurements, to mimic field soil–water dynamics. Water balance components between the two positions on the slope were compared with the goal of identifying differences that might reveal hydrologically driven differences due to LSF paths across the hillslope. The usually considered limitations of these lysimeters, or the borders preventing LSF through the domain, acted as an aid within this installation setup, as the lack of LSF was compensated for through the pumping system at the footslope. The findings from lysimeters were compared with LSF collection system measurements. Weighing lysimeter data indicated that LSF controlled ET_a rates. The results suggest that the onset of LSF contributes to the spatial crop productivity distribution in hillslopes. The present approach may be useful for investigating the impact of LSF on water balance components for similar hillslope sites and crops or other soil surface covers.

Keywords: water balance components; lysimeters; evapotranspiration; lateral subsurface flow; hillslope

1. Introduction

Hillslopes exhibit complex patterns of water storage and transport through space and time, resulting from the interplay between various hydrological processes, including

precipitation, infiltration, runoff, subsurface flow, and actual evapotranspiration (ET_a). The slope inclination, the soil characteristics, the vegetation cover, and the land use practices can all influence hillslope water dynamics [1,2].

Water availability along the hillslope impacts the water status and health of vegetation in both positive and negative ways. For example, wetter soils may support greater plant water availability and thus growth [3]. However, if soils are saturated for extended periods, waterlogging can reduce plant root function due to anaerobic conditions in the root zone [4]. Such conditions occur commonly in certain soil types (such as Stagnosols) [5]. The unfavorable air–water regime of these soils often constrains agricultural production, primarily due to infiltrated water stagnating on or in the poorly permeable subsoil horizons [6].

Climate change is causing changes in the variability of water consumption in agroecosystems, including vineyards [7]. The associated increased temporal variability of rainfall patterns is likely to have a substantial influence on available water and grape production in these systems [8]. Ohana-Levi et al. [9] evaluated seasonal ET_a patterns using lysimeters with vines planted within and showcased the high variability of water consumption throughout the growing seasons. Understanding the complex relationships between climate change, rainfall variability, and vineyard water use is crucial for sustainable viticulture management. Climate change-affected factors, such as intense rainfall events [10], can have significant impacts on soil–water flow dynamics [11]. In particular, higher rain intensities may stimulate infiltration and subsoil water contents, creating conditions for lateral water movement. As a result, variations in soil water availability across a hillslope can arise, with the footslope position potentially exhibiting larger subsoil water amounts than a hilltop.

The plant water status and health changes, as a response to the variable soil moisture conditions at the hillslope, will be reflected in the ET_a fluxes, with ET_a rates increasing with plant water access and plant growth and decreasing where waterlogging impinges plant growth. Thus, a better knowledge of hillslope water dynamics can support improving the productivity of agroecosystems, helping to mitigate the impacts of land use [12] and climate variability [13].

Unfortunately, ET_a fluxes relevant to hillslope-scale water distributions can hardly be observed because, on the one hand, ET_a obtained from footprint-based techniques such as eddy covariance [14] is difficult to downscale, while on the other hand, ET_a obtained from small-scale observation methods such as lysimeters [15] or sap flow sensing [16] is difficult to upscale. An alternative technique could be to use weighing lysimeters, which reproduce field conditions on scales ranging from 0.07 to several square meters and offer high-precision evaluation of the local water balance components. Weighing lysimeters are commonly used in hydrological experiments, but they are not often used in hillslope hydrology research because the separation between the lysimeter and the field soil prevents lateral in- and outflow. State-of-the-art weighing lysimeters are filled monolithically, equipped with a pressure-controlled lower boundary, and allow high-precision and high-temporal-resolution estimation of soil water storage changes and fluxes at the boundaries (i.e., rainfall, drainage, ET_a, or dew) [17]. The lower boundary condition controlled by the dynamic pressure head ensures that lysimeter soil–water dynamics closely correspond with that of the field with respect to upward and downward fluxes [18]. These kinds of lysimeters are used for studying the temporal dynamics of soil water storage [19,20], water and matter budgeting [21–23], and determining seasonal leaching patterns [24], among several other applications [25–30].

The precipitation rate determined by traditional rain gauges (i.e., tipping bucket method) differs from the one obtained by weighing lysimeters and tends to have lower accuracy [31–33]. There are multiple reasons for the deviations in precipitation measurements, including the fact that weighing lysimeters can detect precipitation at the ground surface level without any effect of deformation of the wind field and also of dew, fog, hoar frost, and soil water vapor adsorption [34,35]. Additionally, the data from standard rain gauges are affected by errors due to evaporation, among other factors [36]. Thus, lysimeter

data can contribute to an improved understanding of water cycling [22], water use [37], and the temporal variability of water balance components [38].

Importantly, lysimeters can be placed in different locations in the landscape, such as at the hilltop and footslope of a hillslope, and offer insights into the dynamics of the spatial variability of the water balance components and the soil water flow. Moreover, the usually considered limitations of these lysimeters, or the borders preventing lateral flow through the whole domain, could act as an aid in identifying the impact of hillslope lateral subsurface flow (LSF), as even though flow within the lysimeters is restricted to vertical flow, the controlled lower boundary condition can be influenced by the LSF, and thus by observing the upward fluxes at the footslope, the onset of the LSF could be identified.

This study was carried out at the hilltop and footslope of a hillslope agroecosystem, during the period of 2021–2022, using field hydrological measurements (including weighing lysimeters, soil water content and soil water potential sensors, and LSF collection systems). The aims of the research were (1) to investigate the soil–water dynamics in a hillslope agroecosystem, (2) determine the impact of LSF along the horizon boundaries through quantitative lysimeter measurements (specifically on ET_a), and (3) to compare the lysimeter findings with LSF collection system measurements.

2. Materials and Methods

2.1. Investigated Site Description

The research was carried out at the SUPREHILL Critical Zone Observatory (CZO) (https://sites.google.com/view/suprehill/(accessed on 20 May 2023)) positioned in a hillslope agroecosystem (vineyard) at the experimental station Jazbina (45°51′24″ N, 16°00′22″ E) in Zagreb, Croatia (Figure 1), with a southwest exposition. The rows are oriented downhill, while the inter-row area is grass-covered. The investigated area had an average annual precipitation of 857 mm during the period from 1970 to 2020, along with an air temperature of 11.2 °C.
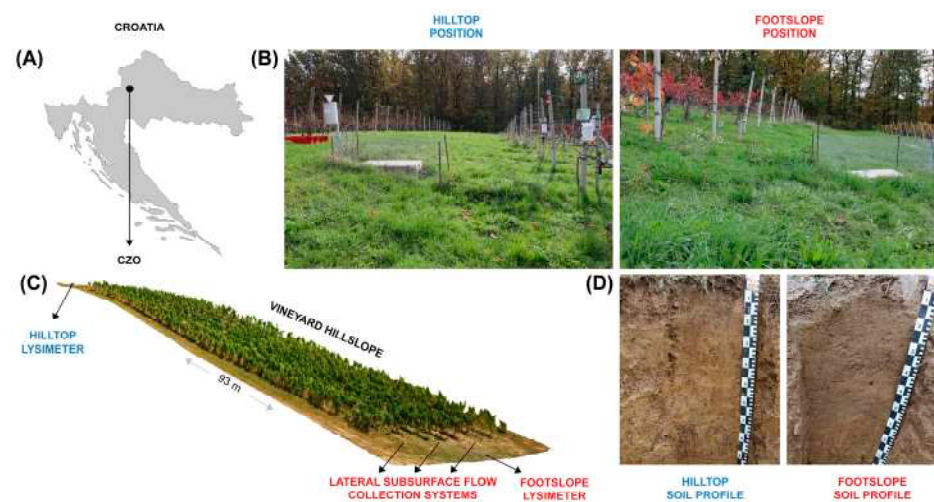
Figure 1. (**A**) Position of the SUPREHILL CZO presented within the borders of Croatia; (**B**) installation positions of weighing lysimeters; (**C**) weighing lysimeter locations and lateral subsurface flow collection systems displayed on a three-dimensional model of the vineyard (produced with UAV data in Agisoft Metashape); (**D**) soil profiles at the installed lysimeter positions.

2.2. Soil Investigation

The disturbed soil samples were obtained at the weighing lysimeter installation position at the hilltop and footslope at 0–30, 30–60, and 60–90 cm soil depths in triplicates to determine the soil particle size distribution and soil organic carbon content (C_{org}). The method of wet sieving and sedimentation (ISO 11277:2020) was used for the soil particle dis-

tribution analysis, while for C$_{org}$ determination, the sulfochromic oxidation (ISO 14235:1998) method was used (Table 1).

Table 1. Average soil particle size distribution and soil organic carbon (C$_{org}$) at the hilltop and footslope position at 0–30, 30–60, and 60–90 cm soil depths and soil type at the SUPREHILL CZO.

Position	Depth	Soil Particle Size (%) [Size in mm]			C$_{org}$	Soil Type (IUSS, 2022)
	(cm)	Sand	Silt	Clay	(g kg^{-1})	
		[2–0.063]	[0.063–0.002]	[<0.002]		
Hilltop lysimeter	0–30	5	79	16	13.3	Dystric Luvic Stagnosol (Aric, Humic, Endoloamic, Episiltic)
	30–60	3	73	24	5.9	
	60–90	6	68	26	2.6	
Footslope lysimeter	0–30	8	76	16	14	Dystric Stagnosol (Aric, Colluvic, Humic, Inclinic, Siltic)
	30–60	7	75	18	9.9	
	60–90	7	69	24	4.1	

The average content (%) of both coarse (2–0.2 mm) and fine (0.2–0.063 mm) sand fractions was low and ranged from 1 to 4%. Both the highest coarse (35%) and fine (44%) silt were found at the hilltop (0–30 cm). Silt content had a decreasing trend with depth at both hilltop and footslope positions. Clay content ranged from 16 % (both hilltop and footslope at 0–30 cm) to 26% (hilltop at 60–90 cm). Contrary to silt, clay had an increasing trend with depth at both hillslope positions. C$_{org}$ ranged from 2.6 g kg^{-1} (footslope at 60–90 cm) to 14.0 g kg^{-1} (footslope at 0–30 cm) and decreased with depth. In this vineyard, the soil type is classified as Dystric (Luvic) Stagnosol by the IUSS Working Group WRB (2022) guidelines [39].

The undisturbed soil samples (soil cores—250 cm^3) have been sampled at two hillslope positions (hilltop/footslope) at weighing lysimeter installation positions in triplicates, at depths 0–20, 20–40, 40–60, and 60–90 cm. The mentioned soil cores were utilized for the estimation of soil hydraulic properties (SHPs) by employing the HYPROP system (the desiccation method) (METER Group, Inc., Pullman, WA, USA) [40] and WP4C (the dew point device) (METER Group, Inc., Pullman, WA, USA) [41]. SHPs were determined using HYPROP-FIT application (METER Group, Inc., Pullman, WA, USA) [42].

Soil hydraulic functions were described using the van Genuchten–Mualem (VGM) single porosity model [43]:

$$\theta(h) = \left\{ \theta_r + \frac{\theta_s - \theta_r}{(1+|\alpha h|^n)^m} \right\} \text{ for } h < 0$$
$$\theta(h) = \theta_s \text{ for } h \geq 0 \tag{1}$$

$$K(h) = K_s S_e^l \left(1 - (1 - S_e^{\frac{1}{m}})^m \right)^2 \tag{2}$$

$$S_e = \frac{\theta - \theta_r}{\theta_s - \theta_r} \tag{3}$$

$$m = 1 - \frac{1}{n}; \ n > 1 \tag{4}$$

where $\theta(h)$ is volumetric water content [L^3 L^{-3}], $K(h)$ is hydraulic conductivity of unsaturated soil at the water pressure head of h [L], θ_r is residual soil water content [L^3 L^{-3}], θ_s is water content at saturation [L^3 L^{-3}], S_e is the effective saturation [-], K_s is the saturated hydraulic conductivity of the soil [L T^{-1}], α is the inverse of air entry value (bubbling pressure) [L^{-1}], n is the dimensionless soil pore size distribution index [-], m is the dimensionless optimization coefficient [-]. The pore connectivity parameter, l, was set to of 0.5, following the recommendations for the majority of soils [44].

Laboratory estimation of SHPs exhibited that θs varied from 0.326 cm^3 cm^{-3}, at the hilltop at 60–90 cm, up to 0.426 cm^3 cm^{-3}, found at the hilltop at 0–20 cm. Ks ranged from 0.277 cm day^{-1}, at the footslope at 40–60 cm, up to 3.86 cm day^{-1}, at the footslope at 60–90 cm. At the hilltop, θs decreased corresponding to the soil depth, while bulk density was increasing, which agrees with past findings at similar research sites [45,46]. Bulk density ranged from 1.46 g cm^{-3} (hilltop at 0–20 cm) to 1.79 g cm^{-3} (hilltop at 60–90 cm). Furthermore, the lowest θs (0.326 cm^3 cm^{-3}) corresponded with the highest bulk density at the site. Values of RMSE (θ) were smaller than 0.02 cm^3 cm^{-3} (Table 2). Soil water retention curves (fitted) were presented in Figure 2.

Table 2. The VGM parameters estimated with HYPROP-FIT. The θ_r is the residual water content, θ_s is the saturated water content, α and n are the empirical retention curve shape parameters, Ks is the saturated hydraulic conductivity, RMSE is the root mean square error, BD is the soil bulk density, and SD is the standard deviation.

Position	Depth [cm]	θ_r [cm^3 cm^{-3}]	θ_s [cm^3 cm^{-3}]	α [cm^{-1}]	n [-]	Ks [cm day^{-1}]	RMSE (θs) [cm^3 cm^{-3}]	RMSE (Ks) [cm day^{-1}]	BD [g cm^{-3}]	SD (BD) [g cm^{-3}]
	0–20	0.0 *	0.426	0.00927	1.238	1.94	0.0097	0.1599	1.46	0.01
Hilltop	20–40	0.06	0.388	0.00426	1.321	0.982	0.0107	0.1626	1.53	0.04
lysimeter	40–60	0.095	0.359	0.00658	1.198	0.847	0.0086	0.3052	1.68	0.03
	60–90	0.129	0.326	0.0178	1.194	1.34	0.0172	0.3257	1.79	0.03
	0–20	0.0 *	0.413	0.00339	1.256	0.277	0.0149	0.1927	1.52	0.07
Footslope	20–40	0.0 *	0.383	0.00629	1.184	0.672	0.0089	0.2311	1.61	0.03
lysimeter	40–60	0.0 *	0.385	0.00831	1.179	0.608	0.012	0.2255	1.55	0.02
	60–90	0.0 *	0.401	0.00718	1.169	3.86	0.0174	0.1088	1.5	0.02

Note: * model assumption was that θ_r values were zero.
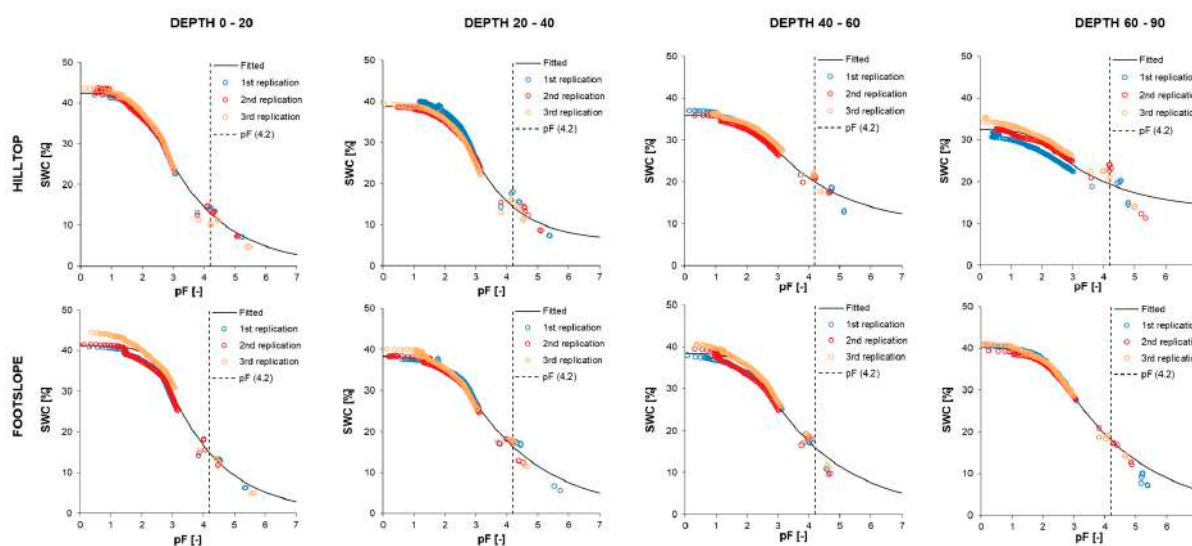
Figure 2. Soil water retention curves (SWRCs) obtained with HYPROP-FIT software (hilltop and footslope positions) at four depths (0–20, 20–40, 40–60, and 60–90 cm) and three replications at the SUPREHILL CZO.

2.3. Weighing Lysimeter Setup, Measurements, Quality Assurance, and Data Processing

At the hilltop and footslope position, high-precision weighing lysimeters (SFL 900, METER Group, Inc., Pullman, WA, USA) [47] were set up by pushing empty lysimeter cylinders (30 cm in diameter, 90 cm long, and with a surface area of 0.07 m^2) vertically into the vineyard cover (grassy area) ground with a centered cutting jack. After the top of the cylinder reached the ground level, the monoliths were excavated and lifted during the installation procedure with a tripod and lifting gear, for the necessary setup and system connections (Figure 3).

Figure 3. Installation procedure of the high-precision weighing lysimeter system at the SUPREHILL CZO: (**A**) vertical downpress of the cylinder during excavation; (**B**) connection of the sensors and system parts; (**C**) lowering of the cylinders below ground level and placement of the drainage tank (field box); (**D**) installation of the central control unit.

The cylinders were placed on continuously measured balances (PL-200, METER Group, Inc. USA) with a measuring precision of 28 g, measuring resolution of 5 g, and high-frequency measurement of a record per minute. Both weighing lysimeters were connected to a central unit that automatically regulates the system and records the data. The lysimeter bottom soil was constantly kept in hydraulic pressure equilibrium with the field soil by using tensiometers (T8, METER Group, Inc. USA) installed in the same 90 cm depth in the immediate surroundings of the lysimeters. Pressure head equilibrium was achieved through a bi-directional pumping system, connected to a pump controller that adjusts the condition at the lysimeter bottom based on the real-time field tensiometer readings. The pressure head in the weighing lysimeter was measured by a pressure sensor in the sensor distribution box, which is connected via a tube to the ceramic surface implemented at the lysimeter bottom. The water from each lysimeter was collected in an external drainage tank, which was placed on a balance (PL-10, METER Group, Inc. USA), with a measuring precision of 1 g, measuring resolution of 0.5 g, and the weight was recorded every minute. Additional sensors were installed inside the lysimeters, measuring soil water content (5TE, METER Group, Inc. USA) and soil matric potential (TEROS 21, METER Group, Inc., Pullman, WA, USA) at 5, 45, and 85 cm soil depth (Figure 4).
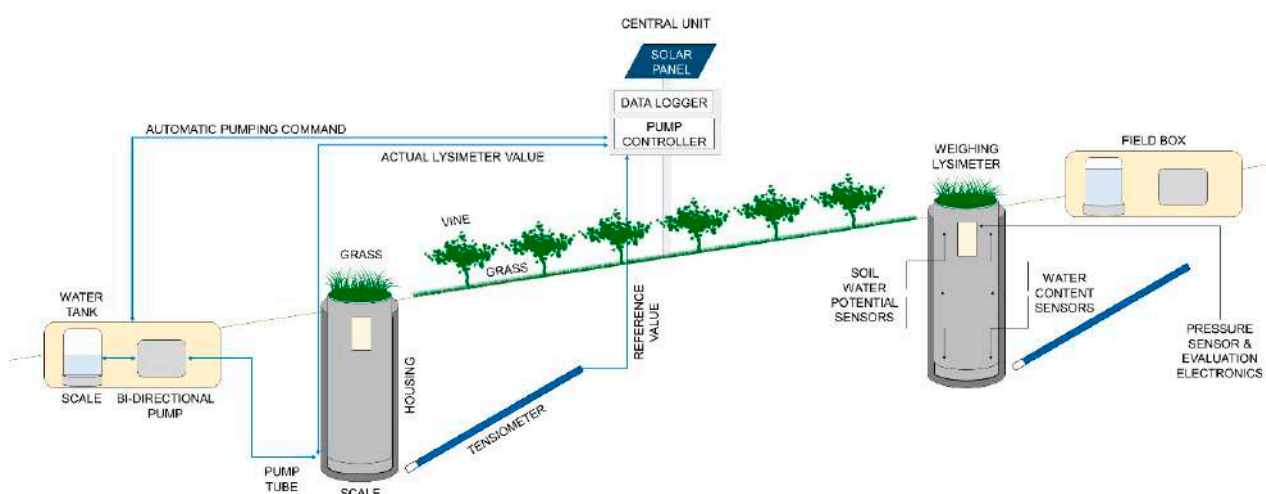
Figure 4. Schematics of the employed setup of the high-precision weighing lysimeters and of the feedback control of the lower hydraulic boundary condition with main components at the SUPREHILL CZO.

To ensure the continuity of the high-interval data records, the operational status of the weighing lysimeters was monitored daily. The screening and examination were conducted in the web application Grafana [48] through automatically transferred data or with examination using daily transferred data on an FTP server. The daily measurements were continuously checked for abnormalities and deviations, to promptly rectify the field causes. Additionally, on a weekly basis, a lysimeter site inspection was carried out.

The collected raw data entries went through manual and automatic plausibility checks. The manual plausibility control was achieved through the procedure of data flagging in DIAdem software (NI, Austin, TX, USA). Flagged data were removed and consequently replaced with an appropriate method specific for the error to compensate for any values that were missing [29,49]. For the gap-filling procedure of ET_a, grass reference evapotranspiration (ET_0) was used. In order to improve the reliability of the data and to smooth the noise, the AWAT filter was employed [50–52]. The AWAT filter applies an adaptive smoothing window size and an adaptive threshold value to lysimeter mass data. The filter has shown to be able to identify even small water fluxes, such as low rates of ET_a or dew formation [52].

The data that were processed were then used to determine ET_a and P from lysimeter weight or mass changes. It was assumed that during each 1 min measurement interval, any lysimeter mass decrease or increase could be attributed to either ET_a or P.

Meteorological data, including air temperature, solar radiation, relative humidity, wind speed, and vapor and air pressure, were derived from a meteo station (ATMOS41, METER Group, Inc., Pullman, WA, USA) set up between the two hillslope positions.

ET_0 was calculated using data from the nearby installed meteorological station and the Penman–Monteith equation [53]:

$$ET_0 = \frac{0.408\Delta(R_n - G) + \gamma\frac{C_n}{T+273}u_2(e_s - e_a)}{\Delta + \gamma(1 + C_d u_2)} \tag{5}$$

where G is the soil heat flux (MJ m^{-2} h^{-1}), Rn is the net radiation (MJ m^{-2} h^{-1}), Δ is the increase in the saturation vapor pressure (MJ m^{-2} h^{-1}), C_d and C_n are constants, γ is the psychrometric constant (kPa C^{-1}), u_2 is the mean hourly wind speed at 2 m height (m s^{-1}), T is the mean hourly temperature (°C), e_a is the mean actual vapor pressure (kPa), and e_s is the saturation vapor pressure (kPa).

Based on the weighing lysimeter data, water storage change (WSC) (mm month^{-1}) was calculated as

$$\text{WSC} = \text{P} - \text{ET}_a - \text{D} + \text{CR} \tag{6}$$

where P is precipitation, including water from rainfall and non-rainfall events (here mainly from dew formation), ET_a is actual evapotranspiration, D is the seepage water, and CR is capillary rise or the upward-directed water from the deeper soil layer (Figure 5).

2.4. Lateral Subsurface Flow Measurements

Self-constructed LSF collection systems were implemented at a soil depth of 60 cm, below the vineyard cover (grassy area), in three vineyard rows closest to the weighing lysimeter (with buffer rows in between) at the identified soil layering transition at the footslope. The collection system was placed on an inclined (2°) aluminum sheet, which served as a water diverter at the installed depth. The diverted water passed through a perforated pipe, coated with a filter net. An upper guard was additionally installed on the instrument, allowing only passing laterally moving water to be collected by the system. Measurements were collected manually on a 14-day basis by pumping out collected soil water through a vertically placed tube from the tank to which the system was connected (Figure 6).
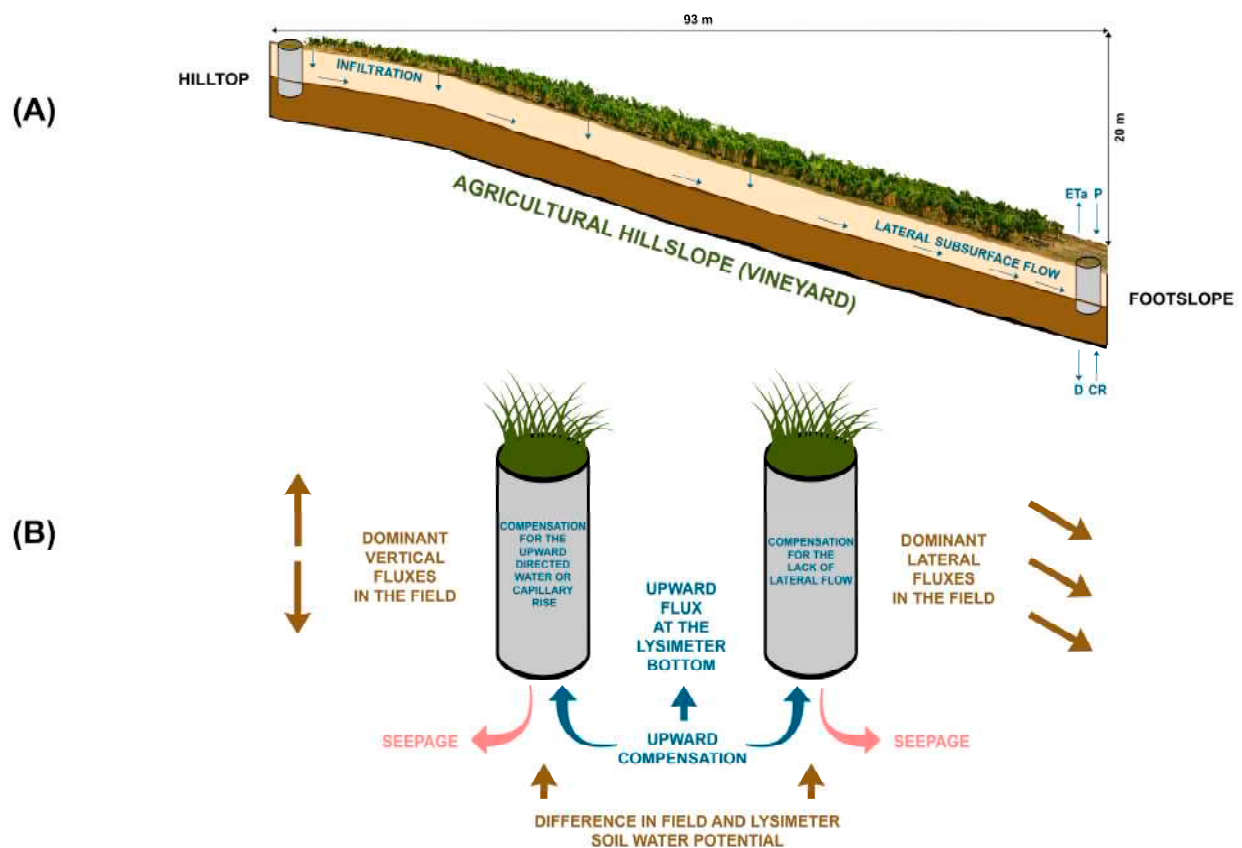
Figure 5. (**A**) Illustration of the investigated water balance components at the hillslope vineyard using the installed lysimeter setup and (**B**) compensational pumping actions at the controlled lower boundary due to differences in field and lysimeter conditions.
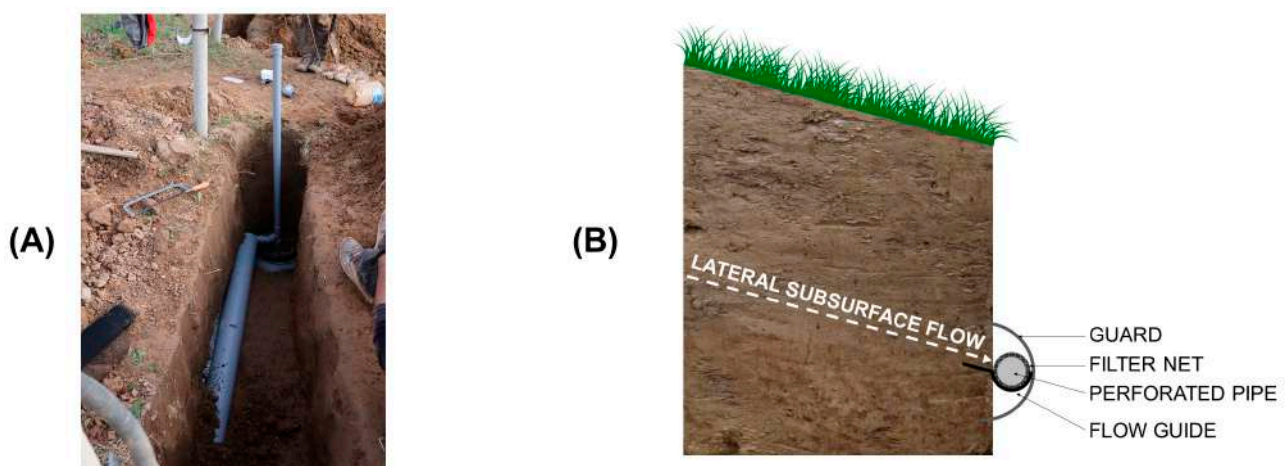
Figure 6. Lateral subsurface flow collection system (**A**) with its cross-section (**B**) installed at the footslope position of the SUPREHILL CZO.

3. Results and Discussion

3.1. Water Balance Components and Change in the Soil Water Storage

Higher average annual precipitation was observed in 2022 (971 mm) than in 2021 (773 mm). The lowest determined monthly precipitation in 2021 was 4.8 mm at the hilltop and 6.7 mm at the footslope in June, while the highest was in May, with 150 mm at the hilltop and 170 mm at the footslope. In 2022, the lowest monthly precipitation was 23.4 mm

at the hilltop and 23.0 mm at the footslope in October, while the highest was in May, with 302 mm at the hilltop and 307 mm at the footslope.

The highest positive water storage changes in 2021 were observed in November, for both hilltop (80.0 mm) and footslope (83.2 mm) following soil rewetting. Moreover, the highest negative water storage changes (hilltop: −165 mm; footslope: −156 mm) were observed in June, the same month with the lowest monthly precipitation (4.8 and 6.7 mm, respectively) and highest monthly ET_a (hilltop: 174; footslope: 199 mm). In 2022, the highest positive water storage changes were observed in September, for both hilltop (198 mm) and footslope (213 mm), the month with the highest precipitation (302 and 307 mm, respectively), while at the hilltop, the highest seepage (64.8 mm) occurred simultaneously. The highest negative water storage change (−60.9 mm) in 2022 occurred in May at the hilltop, while in June of 2022, the highest negative water storage change was observed at the footslope (−99.9 mm), concurrently with the highest ET_a (174 mm) of 2022 for both positions.

In 2021, the highest amount of upward-directed water (53.1 mm) at the footslope occurred in June, while the highest one at the hilltop (39.8 mm) occurred in May. Furthermore, in 2021, the highest seepage at the footslope (37.6 mm) occurred in December, following soil rewetting, while the highest seepage at the hilltop (56.1 mm) occurred in May, concurrently with the highest recorded monthly precipitation (150 mm) in 2021, at the hilltop. For the whole investigated period (2021–2022), the highest upward-directed water amount (75.9 mm) was observed in August of 2022 at the footslope, while the highest case at the hilltop in 2022 (22.2 mm) occurred in April. The highest seepage of 2022 at the hilltop (197.6 mm) was followed by the highest precipitation (302 mm) in September, while the highest seepage at the footslope (72.2 mm) corresponding with the lowest ET_a (36.1 mm) in November (Table 3).

Table 3. Monthly rates of water storage change (WSC), precipitation (P), actual evapotranspiration (ET_a), downward-directed water or seepage (D), and the upward-directed water or capillary rise (CR) calculated for the hilltop and footslope positions in the investigated period (2021–2022) at the SUPREHILL CZO.

Year	Position	[mm]	Jan.	Feb.	Mar.	Apr.	May	June	July	Aug.	Sep.	Oct.	Nov.	Dec.
2021	Hilltop lysimeter	P	60.8	31.8	47.2	72.4	150	4.8	49.5	44.4	26.7	81.2	107	65.5
		ET_a	39.3	52.9	68.5	91.8	134	174	92.7	73.7	52.2	44.3	22.3	25.3
		D	0.0	0.0	0.0	2.9	56.1	7.4	9.1	0.6	0.0	0.0	4.9	37.3
		CR	0.0	0.0	0.0	11.8	39.8	12.1	0.3	0.0	0.0	0.0	0.0	8.2
		WSC	21.6	−21.1	−21.3	−10.5	−0.3	−165	−52.0	−29.9	−25.5	36.9	79.5	11.0
	Footslope lysimeter	P	61.1	24.9	48.6	71.8	170	6.7	54.3	51.5	43.8	92.4	112.7	67.5
		ET_a	42.7	61.5	81.5	116	164	199	130	116	88.5	64.7	29.5	30.5
		D	0.0	0.0	26.9	11.2	18.7	16.5	6.4	1.8	0.0	0.0	0.0	37.6
		CR	0.0	0.0	13.5	11.6	42.2	53.1	32.5	7.9	0.0	0.0	0.0	47.1
		WSC	18.4	−36.6	−46.2	−43.5	29.5	−156	−50.0	−58.4	−44.7	27.7	83.2	46.5
2022	Hilltop lysimeter	P	44.4	42.0	54.5	81.3	49.3	65.6	59.9	31.3	302	23.4	122.2	104
		ET_a	33.6	41.2	67.5	85.2	115	120	71.2	47.4	42.0	50.7	24.4	27.6
		D	7.8	18.6	14.5	45.0	0.5	2.0	0.0	0.0	64.8	16.9	63.0	45.5
		CR	3.5	12.3	14.5	22.2	4.9	3.6	0.0	0.0	2.8	8.2	20.8	0.7
		WSC	6.4	−5.4	−12.9	−26.8	−60.9	−53.1	−11.3	−16.1	198	−35.9	55.6	31.4
	Footslope lysimeter	P	42.2	37.3	50.1	73.8	48.4	65.4	59.4	30.3	307	23.0	121	106
		ET_a	48.8	60.9	90.8	88.0	133	174	149	128	93.4	76.0	36.1	38.7
		D	21.4	16.9	27.0	40.3	30.1	1.2	0.0	9.5	1.8	23.4	72.2	17.0
		CR	13.4	6.0	40.9	23.8	21.5	9.7	38.4	75.9	1.0	56.1	39.2	35.2
		WSC	−14.5	−34.5	−26.8	−30.6	−92.6	−99.9	−50.5	−31.1	213	−20.4	51.6	85.2

The highest lysimeter mass measured at the hilltop was 163.5 kg, while the highest at the footslope was 146.6 kg. The range of mass change for both lysimeters was 22.4 kg.

In 2022, a rapid soil rewetting process is apparent for both lysimeters, as high-volume precipitation events occurred in September, contrary to the prolonged soil rewetting of 2021 (Figure 7).
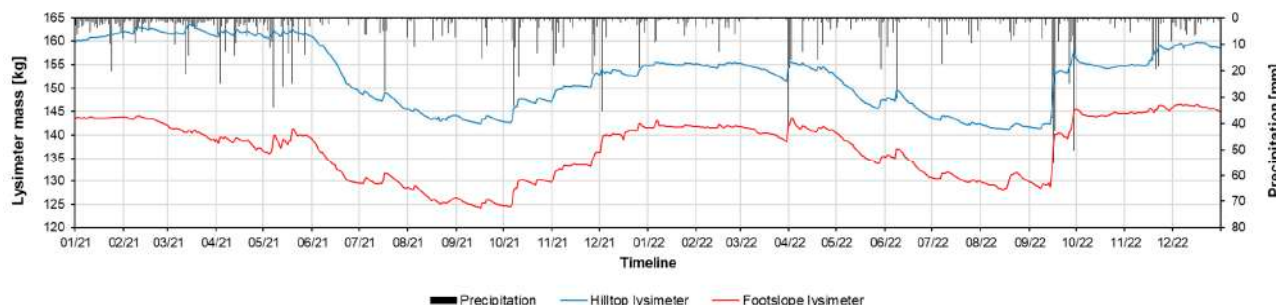
Figure 7. Measured hilltop (blue) and footslope (red) lysimeter mass [kg] and total daily precipitation [mm] in the investigated period (2021–2022) at the SUPREHILL CZO.

*3.2. Field Hydrological Measurements*

During high-volume rainfall events, differences in fluxes at the bottom of the lysimeter can be observed in the form of an oppositional pattern, characterized by a downward flux at the hilltop and an upward flux at the footslope. During such events, water was commonly pumped back into the lysimeter at the footslope position, as the pressure head at the lysimeter bottom was drier compared to the field. The larger difference during such events can be explained by the missing lateral component in the lysimeter. Thus, to compensate for the lack of subsurface lateral inflow across the soil profile at the depth of the lysimeter bottom, water was pumped back into the domain until the lysimeter bottom pressure head was equal to the one in the surrounding field soil (Figure 8).
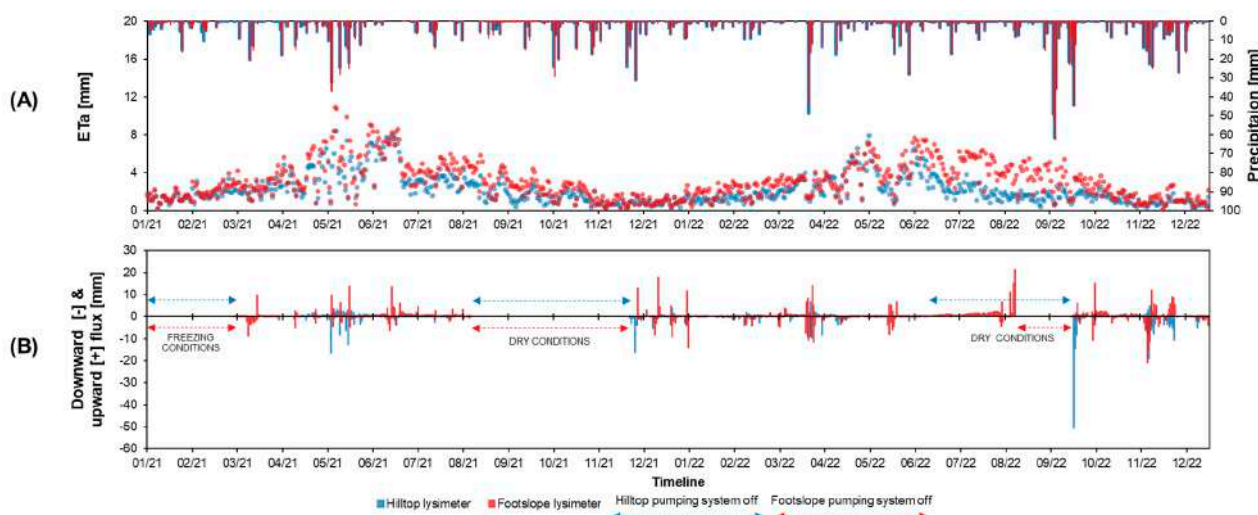
Figure 8. Total daily precipitation [mm], actual evapotranspiration (ET$_a$) [mm] (**A**), and fluxes [mm] (downward [-] representing out; upward [+] representing in) (**B**) at the lysimeter bottom in 2021–2022 at the hilltop (blue) and footslope (red) positions in the investigated period (2021–2022) at the SUPREHILL CZO.

The differences in the lysimeter pumping dynamics between hilltop and footslope can be influenced by LSF. During high-intensity rainfall events (Figure 9A), LSF could lead to increased field soil water potential as compared to the lysimeter bottom at the footslope position (Figure 9B), leading to different mass changes in the drainage tank. Miyazaki [54] demonstrated that LSF can take place at textural boundaries within unsaturated soils that are layered, sloped, and artificially compacted. During high-intensity rainfall events, the

LSF flow rate can increase significantly due to vertically infiltrating water that moves laterally through the soil layers [55] at increased soil moisture. The amount and velocity of LSF are largely determined by the soil's hydraulic properties, such as permeability and water holding capacity, which are in turn influenced by the soil texture differences across the hillslope [6]. Moreover, Montgomery and Dietrich [56] concluded that even though subsurface water saturation can influence LSF routing, the hydrologic response of the steep catchments appeared insensitive to the sloping due to controlling vertically oriented unsaturated flow.
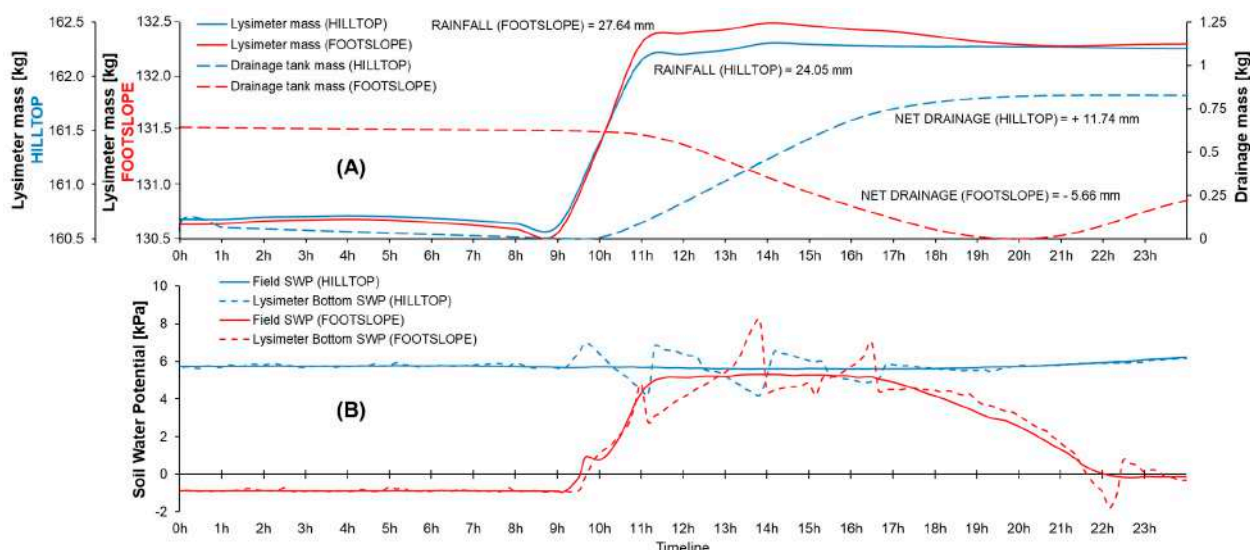
Figure 9. Exemplary changes in lysimeter and drainage tank mass during a rainfall event with field (**A**) and lysimeter bottom soil water potential (SWP) [kPa] (**B**) for the hilltop (blue) and footslope (red) positions measured at the SUPREHILL CZO on 13 May (during the highest-intensity rainfall event recorded in 2021). The mass changes are representative for the 0.07 m^2 of the weighing lysimeter surface.

The onset of LSF was further confirmed by the collection system measurements, installed at the footslope. LSF was generated during or near saturation conditions. During the drying-out phases in both years and until soil rewetting, no LSF was observed. The highest volume of LSF (77.2 L) was captured during prolonged rainfall events in November 2022 during saturated conditions. At the end of the first soil rewetting (December 2021), even though low-rainfall events occurred, the findings suggest that saturated conditions were determinative in LSF onset. These kinds of measurements should be used as means of detecting the signal of flow onset, rather than quantification, due to the difficulties in spatial dimensioning of the captured hillslope flow, in which laboratory experiments and numerical simulations could be more useful. In Figure 10, upward-directed fluxes at the footslope were highlighted (red) in cases of full saturation, showing similar dynamics to those captured by LSF in collection systems, with the exception of periods of pump disengagement due to freezing conditions in the first winter season. If soil water potential reaches a state of zero, the onset of gravitationally driven LSF may occur as the capillary forces become insignificant [57,58]. Furthermore, when observing the whole field soil water potential measurement dataset, dryer soil conditions were apparent in 2021. For the whole investigated period, the correlation between the observed field soil water potential and captured flow was 0.53 (*p*-value < 0.001), contributing to the hypothesis of the LSF onset, while it is suspected that an even better correlation would have been found if the measurements had a higher temporal resolution, as there was often a delay between field measurements from the collection system and saturated conditions (Figure 10). Ehrhardt et al. (2021) [59] compared soil moisture and pressure head observations in the field and within the lysimeter, with a focus on identifying deviations between them. Their analysis revealed that

the field sensors generally responded quicker to rainfall events compared to those in the lysimeter, suggesting the presence of LSF, generated from upper hillslope positions.
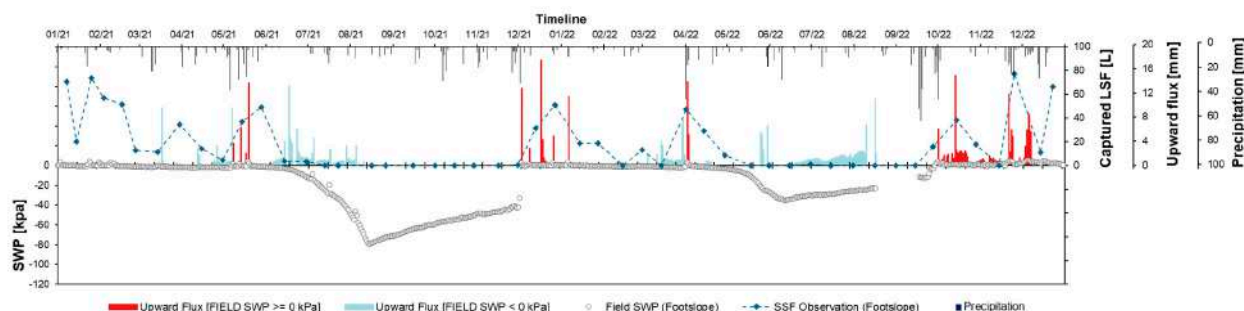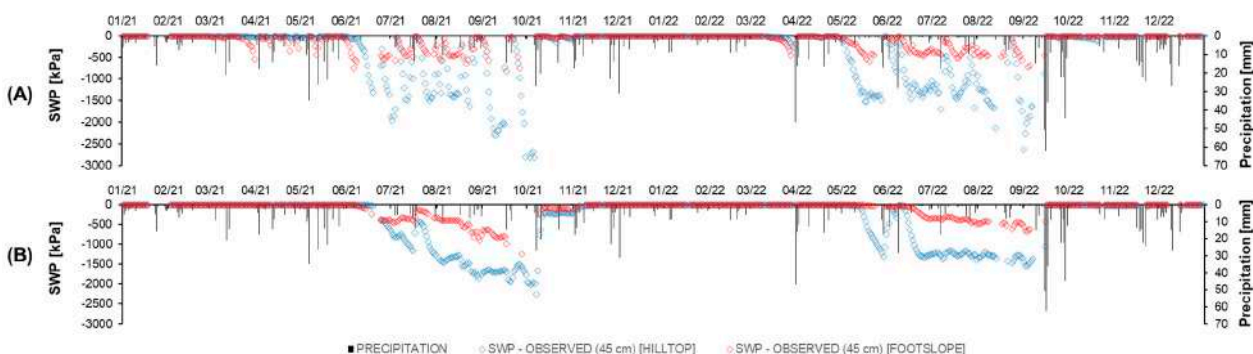

Figure 10. Field soil water potential (SWP) [kPa] (grey), mean captured lateral subsurface flow (LSF) (dark blue) [L], upward flux [mm] (above 0 kPa—red; below 0 kPa—light blue) at the lysimeter bottom, and total daily precipitation (black) measured at the footslope in 2021-2022 at the SUPREHILL CZO.

The soil moisture and soil water potential data demonstrated that higher content of soil water was found at the footslope (Figures 11 and 12). The critical factor of the soil–plant–atmosphere continuum [60] is the availability of water in the soil for plant roots. Root uptake is affected by soil properties [61], soil structure [62], soil organic content [63], and root distribution [64], among other factors. The plant water demand depends on environmental factors such as temperature, humidity, insolation, and wind, which influence ET_a rates [65]. In our case, it is evident that ET_a rates were affected by available soil water.
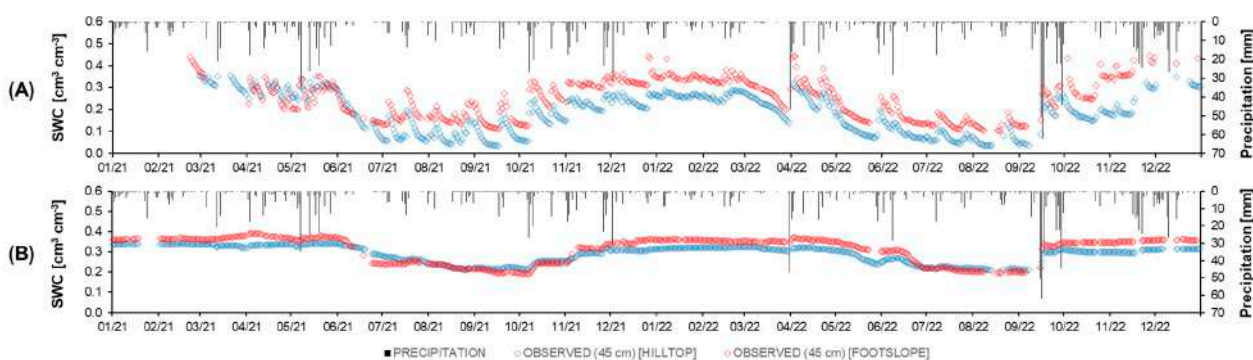
Figure 11. Observed soil water content (SWC) [$cm^3\ cm^{-3}$] at the soil depth of 5 cm (**A**) and 45 cm (**B**) for the hilltop (blue) and footslope (red) position and total daily precipitation [mm] (blue) in the investigated period (2021–2022) at the SUPREHILL CZO.

Figure 12. Observed soil water potential (SWP) [kPa] at 5 cm (**A**) and 45 cm (**B**) soil depth for the hilltop (blue) and footslope (red) and total daily precipitation [mm] (blue) in 2021–2022 at the SUPREHILL CZO.

Long-term and high-precision monitoring is necessary to produce accurate estimations of water balance components [19]. An insight into the impact of LSF-induced soil moisture variations and its effects on the ET_a at varying hillslope positions is valuable information that leads to an improved understanding of hillslope water dynamics. This information can support the productivity of agroecosystems, contributing to sustainable water resource management and conservation [65–67].

4. Conclusions

The high-resolution weighing lysimeters were able to produce reliable data that could be used to identify the effects of lateral subsurface flow (LSF) on the water balance components. The usually considered limitations of these lysimeters (borders preventing lateral flow through the whole domain), within this installation setup acted as an aid in identifying the impact of hillslope LSF. Weighing lysimeter measurement results indicated that the position on the hillslope was determinant in differences caused in water balance components. Moreover, measurements from the LSF collection system helped to confirm this hypothesis.

During high-volume rainfall events, water flux across the lysimeter bottom was often oppositely directed between hilltop (drainage) and footslope (upward-directed water flow). The latter was related to LSF, which ultimately contributed to increased actual evapotranspiration (ET_a) rates. The results suggest that such flow in these periods contributes to the spatial crop productivity distribution in hillslopes. This hypothesis derived from lysimeters at two slope positions should be tested further and compared by more detailed crop observations and modeling tools, using the hillslope as the domain while including field data from outside the lysimeters and in soils along the hillslope.

The results of the water balance components of a hillslope vineyard confirmed that this lysimeter-based approach is transferable to similar hillslope agroecosystems. Long-term and high-precision monitoring of water balance components and state variables is crucial to increase the accuracy of the estimates. Understanding the factors that influence ET_a in the (agro-)ecosystem is crucial for sustainable water resource management and conservation.

Author Contributions: Conceptualization, V.K., J.G., H.H.G. and V.F; Data curation, V.K. and J.G.; Formal analysis, V.K. and J.G.; Funding acquisition, L.F. and V.F.; Investigation, V.K., J.G., L.F. and V.F.; Methodology, V.K., J.G. and V.F.; Project administration, V.K., L.F. and V.F.; Resources, L.F. and V.F.; Software, V.K., J.G. and J.D.; Supervision, V.F.; Visualization, V.K.; Writing—original draft, V.K.; Writing—review and editing, J.G., L.F., H.H.G., J.D., S.T., M.S., I.B., Z.K., N.R., T.B. and V.F. All authors have read and agreed to the published version of the manuscript.

Institutional Review Board Statement: Not applicable.

Informed Consent Statement: Not applicable.

Data Availability Statement: The data presented in this study are available on demand.

Conflicts of Interest: The authors declare no conflict of interest.

References

1. Mike, K. Hillslope runoff processes and models. *J. Hydrol.* **1988**, *100*, 315–339.
2. Dralle, D.N.; Boisramé, G.F.S.; Thompson, S.E. Spatially variable water table recharge and the hillslope hydrologic response: Analytical solutions to the linearized hillslope Boussinesq equation. *Water Resour. Res.* **2014**, *50*, 8515–8530. [CrossRef]
3. Seneviratne, S.I.; Corti, T.; Davin, E.L.; Hirschi, M.; Jaeger, E.B.; Lehner, I.; Orlowsky, B.; Teuling, A.J. Investigating soil moisture-climate interactions in a changing climate: A review. *Earth-Sci. Rev.* **2010**, *99*, 125–161. [CrossRef]

4. Pan, J.; Sharif, R.; Xu, X.; Chen, X. Mechanisms of Waterlogging Tolerance in Plants: Research Progress and Prospects. *Front. Plant Sci.* **2021**, *11*, 627331. [CrossRef]

5. Ruf, T.; Emmerling, C. The effects of periodically stagnant soil water conditions on biomass and methane yields of *Silphium perfoliatum*. *Biomass Bioenergy* **2022**, *160*, 106438. [CrossRef]

6. Magdić, I.; Safner, T.; Rubinić, V.; Rutić, F.; Husnjak, S.; Filipović, V. Effect of slope position on soil properties and soil moisture regime of Stagnosol in the vineyard. *J. Hydrol. Hydromech.* **2022**, *70*, 62–73. [CrossRef]

7. Droulia, F.; Charalampopoulos, I. A Review on the Observed Climate Change in Europe and Its Impacts on Viticulture. *Atmosphere* **2022**, *13*, 837. [CrossRef]

8. Bois, B.; Pauthier, B.; Brillante, L.; Mathieu, O.; Leveque, J.; Van Leeuwen, C.; Castel, T.; Richard, Y. Sensitivity of grapevine soil-water balance to rainfall spatial variability at local scale level. *Front. Environ. Sci.* **2020**, *8*, 110. [CrossRef]

9. Ohana-Levi, N.; Munitz, S.; Ben-Gal, A.; Netzer, Y. Evaluation of within-season grapevine evapotranspiration patterns and drivers using generalized additive models. *Agric. Water Manag.* **2020**, *228*, 105808. [CrossRef]

10. Noor, M.; Ismail, T.; Shahid, S.; Asaduzzaman, M.; Dewan, A. Projection of rainfall intensity-duration-frequency curves at ungauged location under climate change scenarios. *Sustain. Cities Soc.* **2022**, *83*, 103951. [CrossRef]

11. Si, M.; Guo, X.; Lan, Y.; Fan, B.; Cao, G. Effects of Climatic Variability on Soil Water Content in an Alpine Kobresia Meadow, Northern Qinghai–Tibetan Plateau, China. *Water* **2022**, *14*, 2754. [CrossRef]

12. Yang, X.; Leys, J.; Gray, J.; Zhang, M. Hillslope erosion improvement targets: Towards sustainable land management across New South Wales, Australia. *Catena* **2022**, *211*, 105956. [CrossRef]

13. Arboleda Obando, P.F.; Ducharne, A.; Cheruy, F.; Jost, A.; Ghattas, J.; Colin, J.; Nous, C. Influence of Hillslope Flow on Hydroclimatic Evolution Under Climate Change. *Earths Future* **2022**, *10*, e2021EF002613. [CrossRef]

14. Moorhead, J.E.; Marek, G.W.; Gowda, P.H.; Lin, X.; Colaizzi, P.D.; Evett, S.R.; Kutikoff, S. Evaluation of evapotranspiration from eddy covariance using large weighing lysimeters. *Agronomy* **2019**, *9*, 99. [CrossRef]

15. Kandra, B.; Tall, A.; Gomboš, M.; Pavelková, D. Quantification of Evapotranspiration by Calculations and Measurements Using a Lysimeter. *Water* **2023**, *15*, 373. [CrossRef]

16. Wang, Y.; Horton, R.; Xue, X.; Ren, T. Partitioning evapotranspiration by measuring soil water evaporation with heat-pulse sensors and plant transpiration with sap flow gauges. *Agric. Water Manag.* **2021**, *252*, 106883. [CrossRef]

17. Pütz, T.; Fank, J.; Flury, M. Lysimeters in Vadose Zone Research. *Vadose Zone J.* **2018**, *17*, 4–7. [CrossRef]

18. Groh, J.; Vanderborght, J.; Pütz, T.; Vereecken, H. How to Control the Lysimeter Bottom Boundary to Investigate the Effect of Climate Change on Soil Processes? *Vadose Zone J.* **2016**, *15*, 1–15. [CrossRef]

19. Groh, J.; Vanderborght, J.; Pütz, T.; Vogel, H.-J.; Gründling, R.; Rupp, H.; Rahmati, M.; Sommer, M.; Vereecken, H.; Gerke, H.H. Responses of soil water storage and crop water use efficiency to changing climatic conditions: A lysimeter-based space-for-time approach. *Hydrol. Earth Syst. Sci.* **2020**, *24*, 1211–1225. [CrossRef]

20. Heistermann, M.; Bogena, H.; Francke, T.; Güntner, A.; Jakobi, J.; Rasche, D.; Schrön, M.; Döpper, V.; Fersch, B.; Groh, J.; et al. Soil moisture observation in a forested headwater catchment: Combining a dense cosmic-ray neutron sensor network with roving and hydrogravimetry at the TERENO site Wüstebach. *Earth Syst. Sci. Data* **2022**, *14*, 2501–2519. [CrossRef]

21. Herndl, M.; Pötsch, E.M.; Bohner, A. Lysimeter als Bestandteil eines technischen Versuchskonzeptes zur Simulation der Erderwärmung im Grünland Erderwärmung im Grünland. *Gumpensteiner Lysimetertagung* **2011**, *1*, 119–125.

22. Forstner, V.; Groh, J.; Vremec, M.; Herndl, M.; Vereecken, H.; Gerke, H.H.; Birk, S.; Pütz, T. Response of water fluxes and biomass production to climate change in permanent grassland soil ecosystems. *Hydrol. Earth Syst. Sci.* **2021**, *25*, 6087–6106. [CrossRef]

23. Giraud, M.; Groh, J.; Gerke, H.H.; Brüggemann, N.; Vereecken, H.; Pütz, T. Soil Nitrogen Dynamics in a Managed Temperate Grassland Under Changed Climatic Conditions. *Water* **2021**, *13*, 931. [CrossRef]

24. Brye, K.R.; Daigh, A.L.M.; McMullen, R.L. Seasonal Effects on Leachate Quality from an Ozark Highlands Managed Grassland Using Automated, Equilibrium-Tension Lysimeters. *Vadose Zone J.* **2018**, *17*, 160082. [CrossRef]

25. Ochsner, T.E.; Schumacher, T.W.; Venterea, R.T.; Feyereisen, G.W.; Baker, J.M. Soil Water Dynamics and Nitrate Leaching Under Corn–Soybean Rotation, Continuous Corn, and Kura Clover. *Vadose Zone J.* **2018**, *17*, 1–11. [CrossRef]

26. Kupfersberger, H.; Klammler, G.; Schumann, A.; Brückner, L.; Kah, M. Modeling Subsurface Fate of S -Metolachlor and Metolachlor Ethane Sulfonic Acid in the Westliches Leibnitzer Feld Aquifer. *Vadose Zone J.* **2018**, *17*, 170030. [CrossRef]

27. Torrentó, C.; Prasuhn, V.; Spiess, E.; Ponsin, V.; Melsbach, A.; Lihl, C.; Glauser, G.; Hofstetter, T.B.; Elsner, M.; Hunkeler, D. Adsorbing vs. Nonadsorbing Tracers for Assessing Pesticide Transport in Arable Soils. *Vadose Zone J.* **2018**, *17*, 170033. [CrossRef]

28. Briones, M.J.I.; Ineson, P.; Poskitt, J. Climate change and *Cognettia sphagnetorum*: Effects on carbon dynamics in organic soils. *Funct. Ecol.* **1998**, *12*, 528–535. [CrossRef]

29. Groh, J.; Slawitsch, V.; Herndl, M.; Graf, A.; Vereecken, H.; Pütz, T. Determining dew and hoar frost formation for a low mountain range and alpine grassland site by weighable lysimeter. *J. Hydrol.* **2018**, *563*, 372–381. [CrossRef]

30. Groh, J.; Pütz, T.; Gerke, H.H.; Vanderborght, J.; Vereecken, H. Quantification and Prediction of Nighttime Evapotranspiration for Two Distinct Grassland Ecosystems. *Water Resour. Res.* **2019**, *55*, 2961–2975. [CrossRef]

31. Haselow, L.; Meissner, R.; Rupp, H.; Miegel, K. Evaluation of precipitation measurements methods under field conditions during a summer season: A comparison of the standard rain gauge with a weighable lysimeter and a piezoelectric precipitation sensor. *J. Hydrol.* **2019**, *575*, 537–543. [CrossRef]

32. Hoffmann, M.; Schwartengräber, R.; Wessolek, G.; Peters, A. Comparison of simple rain gauge measurements with precision lysimeter data. *Atmos. Res.* **2016**, *174–175*, 120–123. [CrossRef]
33. Herbrich, M.; Gerke, H.H. Autocorrelation analysis of high resolution weighing lysimeter time series as a basis for determination of precipitation. *J. Plant Nutr. Soil Sci.* **2016**, *179*, 784–798. [CrossRef]
34. Schnepper, T.; Groh, J.; Gerke, H.H.; Reichert, B.; Pütz, T. Evaluation of precipitation measurement methods using data from precision lysimeter network. *Hydrol. Earth Syst. Sci. Discuss.* **2022**, 1–33. [CrossRef]
35. Kohfahl, C.; Molano-Leno, L.; Martínez, G.; Vanderlinden, K.; Guardiola-Albert, C.; Moreno, L. Determining groundwater recharge and vapor flow in dune sediments using a weighable precision meteo lysimeter. *Sci. Total Environ.* **2019**, *656*, 550–557. [CrossRef]
36. Graf, A.; Bogena, H.; Drüe, C.; Hardelauf, H.; Pütz, T.; Heinemann, G.; Vereecken, H. Spatiotemporal relations between water budget components and soil water content in a forested tributary catchment. *Water Resour. Res.* **2014**, *50*, 4837–4857. [CrossRef]
37. Beeson, R.C. Weighing lysimeter systems for quantifying water use and studies of controlled water stress for crops grown in low bulk density substrates. *Agric. Water Manag.* **2011**, *98*, 967–976. [CrossRef]
38. Brown, S.; Wagner-Riddle, C.; Debruyn, Z.; Jordan, S.; Berg, A.; Ambadan, J.T.; Congreves, K.A.; Machado, P.V.F. Assessing variability of soil water balance components measured at a new lysimeter facility dedicated to the study of soil ecosystem services. *J. Hydrol.* **2021**, *603*, 127037. [CrossRef]
39. International Union of Soil Sciences (IUSS) Working Group WRB. *International Soil Classification System for Naming Soils and Creating Legends for Soil Maps*, 4th ed.; IUSS: Vienna, Austria, 2022; ISBN 9798986245119.
40. METER. *HYPROP Manual*; UMS: Munich, Germany, 2015.
41. METER. *WP4C Manual*; METER: Pullman, WA, USA, 2021.
42. METER. *HYPROP-FIT User's Manual*; METER: Pullman, WA, USA, 2015.
43. Van Genuchten, M.T. A closed-form equation for predicting the hydraulic conductivity of unsaturated soils. *Soil Sci. Soc. Am. J.* **1980**, *44*, 892–898. [CrossRef]
44. Mualem, Y. A New Model for Predicting the Hydraulic Conductivity of Unsaturated Porous Media. *Water Resour. Res.* **1976**, *12*, 513–522. [CrossRef]
45. Kanso, T.; Tedoldi, D.; Gromaire, M.C.; Ramier, D.; Saad, M.; Chebbo, G. Horizontal and vertical variability of soil hydraulic properties in roadside sustainable drainage systems (SuDS)-nature and implications for hydrological performance evaluation. *Water* **2018**, *10*, 987. [CrossRef]
46. Kool, D.; Tong, B.; Tian, Z.; Heitman, J.L.; Sauer, T.J.; Horton, R. Soil water retention and hydraulic conductivity dynamics following tillage. *Soil Tillage Res.* **2019**, *193*, 95–100. [CrossRef]
47. METER. *Group AG Smart Field Lysimeter—User's Manual*; METER: Pullman, WA, USA, 2019.
48. Grafana Labs. *Grafana Documentation*, version 9.2.4; Grafana Labs: New York, NY, USA, 2023.
49. Pütz, T.; Kiese, R.; Wollschläger, U.; Groh, J.; Rupp, H.; Zacharias, S.; Priesack, E.; Gerke, H.H.; Gasche, R.; Bens, O.; et al. TERENO-SOILCan: A lysimeter-network in Germany observing soil processes and plant diversity influenced by climate change. *Environ. Earth Sci.* **2016**, *75*, 1242. [CrossRef]
50. Peters, A.; Nehls, T.; Schonsky, H.; Wessolek, G. Separating precipitation and evapotranspiration from noise—A new filter routine for high-resolution lysimeter data. *Hydrol. Earth Syst. Sci.* **2014**, *18*, 1189–1198. [CrossRef]
51. Peters, A.; Nehls, T.; Wessolek, G. Technical note: Improving the AWAT filter with interpolation schemes for advanced processing of high resolution data. *Hydrol. Earth Syst. Sci.* **2016**, *20*, 2309–2315. [CrossRef]
52. Peters, A.; Groh, J.; Schrader, F.; Durner, W.; Vereecken, H.; Pütz, T. Towards an unbiased filter routine to determine precipitation and evapotranspiration from high precision lysimeter measurements. *J. Hydrol.* **2017**, *549*, 731–740. [CrossRef]
53. Allen, R.G.; Pruitt, W.O.; Wright, J.L.; Howell, T.A.; Ventura, F.; Snyder, R.; Itenfisu, D.; Steduto, P.; Berengena, J.; Yrisarry, J.B.; et al. A recommendation on standardized surface resistance for hourly calculation of reference ETo by the FAO56 Penman-Monteith method. *Agric. Water Manag.* **2006**, *81*, 1–22. [CrossRef]
54. Miyazaki, T. Water flow in unsaturated soil in layered slopes. *J. Hydrol.* **1988**, *102*, 201–214. [CrossRef]
55. Scherrer, S.; Naef, F.; Fach, A.O.; Cordery, I. Formation of runoff at the hillslope scale during intense precipitation. *Hydrol. Earth Syst. Sci.* **2007**, *11*, 907–922. [CrossRef]
56. Montgomery, D.R.; Dietrich, W.E. Runoff generation in a steep soil-mantled landscape. *Water Resour. Res.* **2002**, *38*, 1168. [CrossRef]
57. Lu, N.; Kaya, B.S.; Godt, J.W. Direction of unsaturated flow in a homogeneous and isotropic hillslope. *Water Resour. Res.* **2011**, *47*, 1–15. [CrossRef]
58. Lv, M.; Hao, Z.; Liu, Z.; Yu, Z. Conditions for lateral downslope unsaturated flow and effects of slope angle on soil moisture movement. *J. Hydrol.* **2013**, *486*, 321–333. [CrossRef]
59. Ehrhardt, A.; Groh, J.; Gerke, H.H. Wavelet analysis of soil water state variables for identification of lateral subsurface flow: Lysimeter vs. field data. *Vadose Zone J.* **2021**, *20*, 1–24. [CrossRef]
60. Norman, J.M.; Anderson, M.C. *Soil-Plant-Atmosphere Continuum*; Elsevier: Amsterdam, The Netherlands, 2005; Volume 4, ISBN 9780080547954.
61. Dodd, M.B.; Lauenroth, W.K. The influence of soil texture on the soil water dynamics and vegetation structure of a shortgrass steppe ecosystem. *Plant Ecol.* **1997**, *133*, 13–28. [CrossRef]

62. Ojeniyi, S.O.; Dexter, A.R. Effect of soil structure on soil water status. *Soil Tillage Res.* **1984**, *4*, 371–379. [CrossRef]
63. Rattan, L. Soil organic matter and water retention. *Agron. J.* **2020**, *21*, 3265–3277. [CrossRef]
64. Akuraju, V.R.; Ryu, D.; George, B. Estimation of root-zone soil moisture using crop water stress index (CWSI) in agricultural fields. *GISci. Remote Sens.* **2021**, *58*, 340–353. [CrossRef]
65. Bhatt, R.; Hossain, A. Concept and Consequence of Evapotranspiration for Sustainable Crop Production in the Era of Climate Change. In *Advanced Evapotranspiration Methods and Applications*; IntechOpen: London, UK, 2019. [CrossRef]
66. Duffkov, R. Influence of Soil Physical Properties and Terrain Relief on Actual Evapotranspiration in the Catchment with Prevailing Arable Land Determined by Energy Balance and Bowen Ratio. In *Evapotranspiration—An Overview*; IntechOpen: London, UK, 2013. [CrossRef]
67. Zou, M.; Niu, J.; Kang, S.; Li, X.; Lu, H. The contribution of human agricultural activities to increasing evapotranspiration is significantly greater than climate change effect over Heihe agricultural region. *Sci. Rep.* **2017**, *7*, 8805. [CrossRef]